UV Laser Photoactivation of Hexachloroplatinate Bound to Individual Nucleobases in Vacuo as Molecular Level Probes of a Model Photopharmaceutical

Edward Matthews, Ananya Sen, Naruo Yoshikawa, Ed Bergström and Caroline E. H. Dessent*

Department of Chemistry, University of York, Heslington, York, YO10 5DD, UK.

*Corresponding Author: Fax: 44-1904-322516. E-mail: caroline.dessent@york.ac.uk

ABSTRACT

Isolated molecular clusters of adenine, cytosine, thymine and uracil bound to hexachloroplatinate, $PtCl_6^{2-}$, have been studied using laser electronic photodissociation spectroscopy to investigate photoactivation of a platinum complex in the vicinity of a nucleobase. These metal complex-nucleobase clusters represent model systems for identifying the fundamental photochemical processes occurring in photodynamic platinum drug therapies that target DNA. This is the first study to explore the specific role of a strongly photoactive platinum compound in the aggregate complex. Each of the clusters studied displays a broadly similar absorption spectra, with a strong λ_{max} ~4.6 eV absorption band and a subsequent increase in the absorption intensity towards higher spectral-energy. The absorption bands are traced to ligand-to-metal-charge-transfer excitations on the $PtCl_6^{2-}$ moiety within the cluster, and result in Cl^-·nucleobase and $PtCl_5^-$ as primary photofragments. These results demonstrate how selective photoexcitation can drive distinctive photodecay channels for a model photo-pharmaceutical. In addition, cluster absorption due to excitation of nucleobase-centred

chromophores is observed in the region around 5 eV. For the uracil cluster, photofragments consistent with ultrafast decay of the excited state and vibrational predissociation on the ground-state surface are observed. However, this decay channel becomes successively weaker on going from thymine to cytosine to adenine, due to differential coupling of the excited states to the electron detachment continuum. These effects demonstrate the distinctive photophysical characteristics of the different nucleobases, and are discussed in the context of the recently recorded photoelectron spectra of theses clusters.

KEYWORDS

Nucleobase photochemistry
Multiply charged anions
Nucleobase photophysics
Laser spectroscopy
Photodynamic Therapy
Pt complex photoactivation

1. INTRODUCTION

Photoactive metallodrugs are the subject of intense current investigation as potential chemotherapy treatments.[1] These compounds can frequently act as "prodrugs" which are compounds that have low native toxicity but can be selectively activated in diseased tissue.[2] A number of platinum compounds have been shown to have considerable potential as anti-cancer prodrugs since they become highly cytotoxic upon photoactivation.[3] While the anti-cancer potential of such compounds has been demonstrated through *in vitro* investigations, many questions exist regarding the key photophysical and photochemical processes that take place in the complex biological medium.[3,4]

In a recent series of studies, we have used electrospray ionization to produce nucleobase-platinum complex clusters as isolated gas-phase molecular aggregates.[5-7] The study of such clusters in the gas-phase has considerable potential to contribute to our understanding of the factors that affect metal-compound-nucleobase binding within a well-defined, controlled environment, whilst also allowing the characterisation of the photophysics and photochemistry of the aggregates via laser spectroscopy. Our initial work involved $Pt(CN)_4^{2-}$ and $Pt(CN)_6^{2-}$ as simple, model Pt(II/IV) complexes, bound to the DNA nucleobases thymine, cytosine and adenine along with the RNA nucleobase, uracil. The $Pt(CN)_4^{2-}$ and $Pt(CN)_6^{2-}$ complexes do not display strong chromophores across the 220-300 nm range studied, hence allowing us to focus in those initial studies on photoexcitation of the nucleobase-centred chromophore. In this work, we investigate aggregates consisting of the same series of nucleobases this time bound to the hexachloroplatinate complex ($PtCl_6^{2-}$), to allow us to study the effect of including a "photoactive" Pt complex within the aggregate cluster, hence moving towards more pharmaceutically relevant model systems.

The intrinsic UV spectroscopy of isolated, gas-phase hexachloroplatinate has been investigated in detail by Weber and co-workers using photodissociation spectroscopy.[8] This study revealed that photoexcitation of $PtCl_6^{2-}$ results in ionic fragmentation of the dianion into $PtCl_5^-$ and Cl^-, with a band profile that peaks at 4.55 eV. $PtCl_4^-$ was also observed as a photofragment through this band, and then as an increasingly intense photofragment to higher excitation energy. It was concluded that the $PtCl_4^-$ is produced from the initially formed $PtCl_5^-$ due to excess energy residing in the molecule following ionic fragmentation of the initial dianion. Photodetachment (*i.e.* production of $PtCl_6^-$) is also prominent, with excitation of electronic transitions of the dianion leading to resonant enhancement of the photodetachment cross-section superimposed on direct electron detachment above the electron detachment

threshold (~3.75 eV). Wang and Wang have used photoelectron spectroscopy to characterize the electron detachment properties of gas-phase hexachloroplatinate.[9] There have also been several high-level theoretical studies of gaseous $PtCl_6^{2-}$.[10,11] Therefore, the intrinsic properties of the $PtCl_6^{2-}$ dianion are well established in the gas-phase.

The photochemical activity of the $PtCl_6^{2-}$ complex has been very extensively studied in the solution phase as a prototype transition metal complex.[12] While the earliest such measurements were conducted around 200 years ago, there is considerable current work in this field due to the applications of $PtCl_6^{2-}$ in the photoproduction of platinum nanoparticles and in the modification of the surfaces of TiO_2 and CdS to produce tailored photocatalysts.[13-15]

UV light has the potential to effect permanent damage in the structure of DNA, so that the UV photophysics and photochemistry of DNA is of considerable fundamental importance. Since the nucleobase units of DNA are responsible for absorbing UV light, their photophysical properties have been very widely studied. Nucleobases are known to display ultrafast non-radiative decay following UV excitation, which converts the electronic excitation into heat energy which can be dissipated on the ground electronic state. References 16-18 provide reviews of experimental work in this extensive field, while Reference 19 provides a very recent review of associated theoretical studies.

We have recently studied the low-temperature photoelectron spectra of clusters of $PtCl_6^{2-}$ bound to individual nucleobases as a precursor to the current study.[20] Adiabatic electron detachment energies and repulsive Coulomb barriers were obtained, providing us with electron detachment energies to aid the interpretation of the photodissociation spectra presented below. The photoelectron spectra of the $PtCl_6^{2-}$·nucleobase clusters displayed well-resolved, distinct peaks that are consistent with structures where the $PtCl_6^{2-}$ dianion is largely unperturbed. This is important as it illustrates that the precursor clusters to be studied in this work contain each of the component moieties as intact molecules.

2. EXPERIMENTAL AND THEORETICAL METHODS

Experiments were performed using a Bruker AmaZon Ion Trap mass spectrometer. Typical instrumental parameters were; nebulising gas pressure of 10.0 psi; injection rate of 250 μL/hr; drying gas flow rate of 8.0 L min^{-1}; capillary temperature of 100ºC; and ion isolation time of 40 ms. The nucleobase-hexachloroplatinate complexes were prepared by electrospraying solutions of the nucleobase and the dianion (Na_2PtCl_6 at $1x10^{-4}$ mol dm^{-3} mixed with droplets of the nucleobase solutions at $1x10^{-2}$ mol dm^{-3}) in deionised water. (No experiments were

conducted for guanine, due to its low solubility in water.) All chemicals were purchased from Sigma Aldrich and used without further purification. Fragment ions with m/z less than ~50 are not detectable in the instrument since low masses fall outside of the mass window of the trap.

Low-energy collision induced dissociation (CID) (also termed *resonance excitation*) was performed on isolated ions by applying an excitation AC voltage to the end caps of the trap to induce collisions of the trapped anionic complexes with the He buffer gas. We have described these experiments in detail previously,[21,22] and we refer the reader to these references for further details and a discussion of the limitations of CID experiments for obtaining quantitative information. UV laser photo-fragmentation experiments were conducted in the AmaZon ion-trap mass spectrometer, which was modified for the laser experiments as described in detail in Section S1 of the Supplementary Information (SI). All experiments were run under one-photon conditions, by ensuring that the photodepletion intensity increases linearly with laser power at several points across the scanned spectral region.

Time-dependent density functional theory (TD-DFT) calculations were carried out to aid the interpretation of the experimental spectra. TD-DFT have been successfully applied to nucleobases, nucleobase clusters and platinum complexes previously, allowing us to reliably apply these calculations to aid the assignment of electronic transitions.[23-25] The TD-DFT calculations all use the optimized cluster geometries that have been published previously in Ref. 20. Gaussian 09 was used for all calculations,[26] employing the M06-2X functional with the split basis set of: 6-311+G(2d,2p) on all first and second row atoms and the Def2-TZVPP (from Aldrich et al, triple zeta valence basis set with additional polarization functions) basis set to describe the platinum valence orbitals with the 60 core electrons represented by the Stuttgart/Dresden electron core pseudopotential, at the Wood-Boring quasi-relativistic level of theory.[27-29] The def2-TZVPP basis set has previously been used successfully to describe the valence electrons of $PtCl_6^{2-}$ in TD-DFT calculations.[8]

3. RESULTS AND DISCUSSION

3.1 Low-energy collisional activation of the $PtCl_6^{2-}$-nucleobase clusters

The negative ion electrospray mass spectrum (ESI-MS) of a mixed $PtCl_6^{2-}$/thymine solution is displayed in Fig. 1. While the $PtCl_6^{2-}$ dianion dominates the ESI-MS, peaks resulting from clusters of $PtCl_6^{2-}$ with one and two nucleobases are also clearly visible *i.e.* $PtCl_6^{2-}{\cdot}T_n$ n = 1, 2. The propensity for the solution components to react is evident from the prominent appearance of several other species in the ESI-MS including the deprotonated nucleobase anion $[T\text{-}H]^-$, the $T{\cdot}Cl^-$ cluster, $PtCl_x^-$ (x = 3 – 5) complex ions, and the peaks centred at ~ m/z =192, 354 and

390 mass units which have a chloride ligand of a $PtCl_x$ complex replaced by water or hydroxide. The rich chemistry evident in the $PtCl_6^{2-}$/thymine mass spectrum contrasts with the much simpler ESI-MS observed for mixtures of thymine with $Pt(CN)_6^{2-}$ and $Pt(CN)_4^{2-}$.[5] Similar mass spectra were observed when solutions of the other nucleobases with $PtCl_6^{2-}$ were electrosprayed.

Low-energy CID was performed for the $PtCl_6^{2-}\cdot M$, M = A, C, T, U clusters, with Table 1 summarising the results. Fig. 2 displays the % fragmentation curves across the collisional activation range. We note that the precursor cluster ions are stable across the low-energy CID range, illustrating that they are stable ground-state molecular clusters and do not undergo metastable decay prior to resonance excitation.[21] The major fragmentation process for each of the $PtCl_6^{2-}\cdot M$ clusters is simple cluster fission, consistent with an initial cluster that is composed of intact $PtCl_6^{2-}$ and nucleobase units:

$$PtCl_6^{2-}\cdot M \rightarrow PtCl_6^{2-} + M \quad [1]$$

In addition, each of the $PtCl_6^{2-}\cdot M$ clusters also fragments via a chloride ion transfer reaction:

$$PtCl_6^{2-}\cdot M \rightarrow PtCl_5^{-} + M\cdot Cl^{-} \quad [2]$$

This reaction can be viewed as an "ionic fragmentation" reaction of the multiply charged cluster.[21] Reaction [2] is most prominent for the $PtCl_6^{2-}\cdot A$ cluster and least prominent for the $PtCl_6^{2-}\cdot T$ cluster. (The origin of the difference in the fragmentation characteristics may lie in the different structures of systems. Adenine does not contain an electron rich carbonyl whereas $PtCl_6^{2-}\cdot T$ has a carbonyl close to the chloride ligands.) In addition to fragmentation reactions [1] and [2], the deprotonated nucleobase, i.e. $[M-H]^-$, is observed as a very low intensity fragment from $PtCl_6^{2-}\cdot A$ and $PtCl_6^{2-}\cdot U$. Isolation of the $A\cdot Cl^-$ cluster and subsequent CID produced the deprotonated nucleobase as the sole fragment ion,

$$M\cdot Cl^{-} \rightarrow [M-H]^{-} + HCl \quad [3]$$

indicating that the deprotonated nucleobase fragments can be formed via a two stage process from the $PtCl_6^{2-}\cdot M$ cluster. The low intensity of $[M-H]^-$ as a direct CID product from excitation of the $PtCl_6^{2-}\cdot M$ clusters is intriguing given that $[M-H]^-$ appears so prominently in the ESI-MS. This suggests that $[M-H]^-$ is probably formed via solution-phase reactions prior to electrospray.

In summary, the low-energy CID measurements of the $PtCl_6^{2-}\cdot M$ clusters provide further evidence that the clusters are composed of intact $PtCl_6^{2-}$ and nucleobase moieties. The clusters all display similar binding energies (as reflected by the similar $E_{1/2}$ values in Table 1), and decay of the clusters on the ground-state potential energy surface results predominantly in formation of $PtCl_6^{2-}$.

3.2 Time-dependent Density Functional Theory Calculations of the $PtCl_6^{2-}$-nucleobase clusters

Fig. 3 shows a TD-DFT calculated excitation spectrum of the $PtCl_6^{2-}$·U cluster, with the associated excitation assignments being listed in Table 2. The calculated spectrum of $PtCl_6^{2-}$·U is presented in the main text, with results for the other $PtCl_6^{2-}$·M clusters (and $PtCl_6^{2-}$) given in the SI. TD-DFT calculations of uncomplexed $PtCl_6^{2-}$ have been performed previously with the PBE0 functional,[8] producing a calculated UV spectrum with weak and strong bands (I and II) at 4.74 and 6.19 eV, respectively, both associated with ligand to metal charge transfer (LMCT) transitions. Calculations on $PtCl_6^{2-}$ using the M06-2X functional were also conducted as part of this work to allow direct comparison to the cluster calculations, with bands I and II appearing at 4.59 and 5.98 eV, respectively

The calculated UV spectrum of $PtCl_6^{2-}$·U (Fig. 3) is blue-shifted compared to bare $PtCl_6^{2-}$, with bands I and II appearing at 4.73 and 6.10 eV. Analysis of the molecular orbitals involved in the bright excitations (oscillator strength > 0.005) over the experimental range reveals transitions from a ground-state cluster where the MOs either originate from $PtCl_6^{2-}$ orbitals or from orbitals which have electron density primarily in a uracil π orbital but with minor delocalisation to the $PtCl_6^{2-}$ moiety. The corresponding excited states are localised either on $PtCl_6^{2-}$ orbitals or a uracil π^* orbital (Table 2). While the $PtCl_6^{2-}$ localised transitions are LMCT in nature (as in uncomplexed $PtCl_6^{2-}$), it is evident that complexation with uracil removes degeneracy from these LMCT transitions in the region 4.1 – 4.8 eV,[8] and relaxes the selection rules, such that forbidden transitions in uncomplexed $PtCl_6^{2-}$ at 4.6 – 4.7 eV become allowed. The intense transition at 5.28 eV populates a uracil π^* orbital. This transition occurs close to an experimentally measured and computationally predicted π to π^* transition in gaseous uracil which occurs at ~5.1 eV.[30-32] Gordon and co-workers have performed elegant calculations to probe solvent-induced shifts on the electronic transitions of uracil, and it is evident from these calculations that the gaseous uracil π to π^* transition will shift with sequential solvation.[23]

Similar results were obtained for the other nucleobase clusters (Section S2 of the SI). In general, the clustering of the nucleobase to $PtCl_6^{2-}$ blue-shifts the two LMCT bands such that the peak-to-peak separation is unperturbed relative to bare $PtCl_6^{2-}$. This suggests that the nucleobase primarily interacts to stabilise the ground state of $PtCl_6^{2-}$, and inspection of the MOs reveals that the excited state of both LMCT bands is largely unperturbed by the presence of the nucleobase. Finally, we note that strong nucleobase-centred transitions are seen between

5-5.5 eV for the thymine, cytosine and adenine clusters, analogous to the strong 5.28 eV uracil-centred transition.

3.3 Electronic Laser Photodissociation Spectroscopy of the $PtCl_6^{2-}$ - nucleobase clusters

3.3.1 Photodepletion Spectra of $PtCl_6^{2-}$·M

To explore the $PtCl_6^{2-}$·M UV photochemistry and photophysics, the complexes were photoexcited from 4.0-5.8 eV (310-215 nm). This region begins around the approximate electron detachment energy for each cluster: ~3.96, 3.98, 4.05 and 4.05 eV for M = A, C, T and U, respectively.[20] (We note that since the clusters studied here are dianionic, the electron detachment threshold is given by the repulsive coulomb barrier height added to the electron affinity.) The gas-phase $PtCl_6^{2-}$·M photodepletion (absorption) spectra are presented in Fig. 4. Solution-phase UV-VIS spectra are included in the SI for solution-phase $PtCl_6^{2-}$, as well as the individual solution-phase nucleobases. These spectra can be used along with the TD-DFT calculations to guide the assignment of the gas-phase cluster absorption spectra.[6,7]

All of the photodepletion spectra display broad, non-Gaussian absorption features over the range 4.2-5.2 eV, peaking between 4.44 and 4.63 eV with a maximum at 4.46 eV for adenine; at 4.61 eV for cytosine; between 4.51 and 4.70 eV with a maximum at 4.66 eV for thymine; and at 4.63 eV for uracil. The ~4.6 eV peaks of the $PtCl_6^{2-}$·A and $PtCl_6^{2-}$·T spectra are given as ranges due to the flatness of the depletion profiles in these regions. In addition to the ~4.6 eV peak, each spectrum shows an increase in absorption intensity towards higher photon energies. The spectrum of the cytosine complex also displays a weak absorption feature between 4.0 and 4.2 eV which is not observed in the spectra of the other clusters.

The experimental $PtCl_6^{2-}$·M absorption spectra are in good qualitative agreement with the TD-DFT calculated spectra presented in Sections 3.2 and S2, in that they display a broad feature around 4.6 eV, followed by a rising absorption towards 6 eV, both associated with the LMCT transitions on $PtCl_6^{2-}$. In our previous work on the $Pt(CN)_{4,6}^{2-}$·nucleobase clusters,[5-7] we assigned absorption bands in the 4.7 eV region to nucleobase-centred chromophores, since they have considerably stronger transition intensities than the $Pt(CN)_{4,6}^{2-}$ complexes. However, the solution-phase UV-VIS absorption spectra of the uncomplexed $PtCl_6^{2-}$ and the individual nucleobases indicate that $PtCl_6^{2-}$ displays much more intense excitations across the lower-energy spectral region compared to the nucleobases, and the TD-DFT calculations support this. Therefore, the $PtCl_6^{2-}$ LMCT excitations will dominate, particularly to lower energies, whereas the nucleobase-centred excitations are stronger around 5.2 eV. The photodepletion peak plateaus, observed for $PtCl_6^{2-}$·A and $PtCl_6^{2-}$·T (and $PtCl_6^{2-}$·U and $PtCl_6^{2-}$·C to a lesser extent)

are likely to arise due to the removal of degeneracy in the LMCT absorption of the nucleobase cluster (it is triply degenerate for bare $PtCl_6^{2-}$).

The weak absorption in the cytosine cluster at 4.1 eV is likely the result of the presence a second geometric isomer of this cluster. Two cluster isomers of $PtCl_6^{2-}$·C have been observed in the low-temperature photoelectron spectrum of this cluster, with electron detachment energies of 4.04 eV (minor isomer) and 4.25 eV (major isomer).[20] Thus, photodepletion in the low energy region of the spectrum is enhanced due to photodetachment from the minor isomer. (We note that it is also possible that the absorption in this region of the spectrum is due to transitions of a keto tautomer of cytosine that have been observed previously.[33])

3.3.2 Photofragment Action Spectra of $PtCl_6^{2-}$·M

Fig. 5 presents the photofragment mass spectra of the $PtCl_6^{2-}$·M clusters recorded at 4.77 eV (270 nm), to illustrate the photochemistry that occurs at this excitation energy. The observed photofragments can be classified into two groups, corresponding either to electron detachment processes of the cluster ($PtCl_6^-$, $[PtCl_5(A-H)]^-$, $PtCl_6^-$·A), or to photoinduced cluster dissociation. This classification is based on identifying $PtCl_6^-$·A as an unambiguous electron detachment fragment, and other fragments are labelled as electron detachment fragments if they display an action spectrum profile that mirrors that of $PtCl_6^-$·A. All remaining fragments must then be associated with photoinduced cluster dissociation. When discussing these photoinduced dissociation products, we assume that absorption by either a $PtCl_6^{2-}$ or nucleobase centred-chromophore induces cluster fragmentation following relaxation of the initially populated excited state to a vibrationally excited electronic ground state. This follows either from consideration of the cluster energetics,[34] or from the fact that nucleobase-centred absorptions are known to typically decay on the femtosecond timescale so would not lead to fragmentation in the excited state.[35,36]

The observation of the CID fragments $PtCl_5^-$ and $M{\cdot}Cl^-$ for all clusters, $PtCl_6^{2-}$ for all but the adenine cluster and $[M-H]^-$ for all but the cytosine cluster suggests that fragmentation pathways [1] - [3] are significant following photoexcitation. Production of $PtCl_4^-$ and $PtCl_3^-$ can be attributed to fragmentation of vibrationally excited $PtCl_x^-$ (x = 4, 5, 6) species via the successive loss of Cl radicals, for example:

$$PtCl_5^{-*} \rightarrow PtCl_4^- + Cl\cdot \qquad [4a]$$

$$PtCl_4^{-*} \rightarrow PtCl_3^- + Cl\cdot \qquad [4b]$$

The fragmentation mechanism can be assigned as a successive fragmentation process since no fragments were detected that would accompany $PtCl_3^-$ and $PtCl_4^-$ if fragmentation of the parent

cluster was direct (e.g. Cl_2^-, Cl_3^-, $M{\cdot}Cl_2^-$, or $M{\cdot}Cl_3^-$). A mechanism analogous to [4a] was proposed previously as a pathway to $PtCl_4^-$ in photofragmentation of $PtCl_5^-$.[8] Calculations of the fragmentation reaction energies are included in Section S5 of the SI.

(a) Photofragmentation pathways associated with electron detachment

We now return to discussing the photofragment processes that are associated with electron detachment:

$$PtCl_6^{2-}.M + h\nu \rightarrow PtCl_6^-.M + e^- \qquad [5a]$$

$$PtCl_6^-.M \rightarrow PtCl_6^- + M \qquad [5b]$$

$$PtCl_6^-.M \rightarrow [PtCl_5(M\text{-}H)]^- + HCl \qquad [5c]$$

It is notable that the $PtCl_6^{2-}{\cdot}A$ cluster produces three prominent electron-detachment fragments ($PtCl_6^-$, $PtCl_6^-{\cdot}A$ and $[PtCl_5(A\text{-}H)]^-$), whereas the other $PtCl_6^{2-}{\cdot}M$ clusters produce $PtCl_6^-$ as the sole observed electron detachment fragment. (The $[PtCl_5(A\text{-}H)]^-$ photofragment is discussed in detail in Section S4 of the SI.) It is likely that the different fragmentation pathways seen for the $PtCl_6^{2-}{\cdot}M$ clusters can be traced to the binding energies of the monoanions to the nucleobase within clusters such as $PtCl_6^-{\cdot}A$ and $[PtCl_5(A\text{-}H)]^-$. One possible explanation for this, is the presence of a carbonyl moiety close to the $PtCl_6^-$ binding site for all the nucleobases except adenine (see Ref. 20 for calculated cluster structures); in the monoanionic clusters, long range carbonyl-chloride repulsion may dominate interactions as the short-range hydrogen bonds weaken from the reduction in excess charge. From the $PtCl_6^{2-}{\cdot}A$ photofragment mass spectrum (Figure 5d) it is evident that the relative intensities of $PtCl_6^-$ and $[PtCl_5(A\text{-}H)]^-$ are similar, thus implying that the activation energies for pathways [5b] and [5c] are comparable.

Figure 6 shows the photoproduction spectra for the summed electron detachment fragments across the range 4.0 – 5.8 eV. As would be expected, a gradual increase in photodetachment occurs with increasing photon energy for all the $PtCl_6^{2-}{\cdot}M$ clusters, and this corresponds to an increasing number of electronically excited states of the $PtCl_6^-{\cdot}M$ monoanion. The spectra each have a notable band superimposed on the near-linearly increasing photodetachment cross-section with increasing energy, which peaks between 5.2 and 5.4 eV. This is characteristic of the presence of an excited state, where photoexcitation of this state leads to resonant enhancement of the photodetachment cross-section superimposed on direct electron detachment.[8] It is probable that these excited states are the nucleobase-centred transitions that are expected in this region.

For an electron to become detached from the dianionic $PtCl_6^{2-}$·M complex, it must have sufficient energy to overcome the repulsive coulomb barrier (RCB) for electron detachment as well as the electron binding energy. As discussed above, the photoelectron spectra of the $PtCl_6^{2-}$·M clusters have been measured recently, providing estimates of the detachment thresholds of 3.96 – 4.05 eV.[20] The onset of electron detached fragments in photodissociation spectroscopy provide alternative measurements of the electron detachment thresholds: Inspection of Figure 6 provides values of ~4.0-4.2 eV for the clusters, in line with the estimated values from the photoelectron spectra.

(b) Non-electron detachment photofragmentation pathways

The photofragment mass spectra of the $PtCl_6^{2-}$·M clusters shown in Figure 5 illustrate that the photochemistry of these systems is complex. This can be traced to the fact that each of the components displays chromophores over the spectral region studied, with the $PtCl_6^{2-}$ moiety photodissociating via multiple pathways. To simplify the discussion, we therefore focus on two important facets of the photophysics, namely photochemical products that arise following photoexcitation of the nucleobase chromophore and the photochemical production of Cl^-·M, which should be produced upon excitation of $PtCl_6^{2-}$ centred-chromophores (see below). Our discussion and grouping together of the numerous photofragments is guided by the action spectra, i.e. photofragments that display action spectra with similar profiles are grouped together as they will arise following a common excitation process.

In our recent study of $Pt(CN)_4^{2-}$·M complexes,[5-7] the photochemistry and photophysics of the clusters over the region 220-320 nm were dominated by excitation of the nucleobase-centred chromophore with λ_{max} at ~4.7 eV. The resulting nucleobase-localized excited states appear to undergo ultrafast decay, followed by ergodic decay of the electronic ground state cluster. This gives rise to photofragments that are *identical to the fragments observed upon low-energy CID of the ground state cluster*, both in terms of identity and relative intensity. For the $PtCl_6^{2-}$·M clusters studied in this work, we would expect to see the respective low-energy CID fragments as photofragments across a similar excitation region. Cluster fission, pathway [1], is the major low-energy CID pathway for each of the $PtCl_6^{2-}$·M clusters studied here, with $PtCl_6^{2-}$ being an ionic fragment that is uniquely associated with this dissociation pathway. $PtCl_6^{2-}$ is indeed a significant photofragment for $PtCl_6^{2-}$·U and $PtCl_6^{2-}$·T (Figure 5a and 5b), but appears with lower intensity for $PtCl_6^{2-}$·C (Figure 5c) and is strikingly absent for $PtCl_6^{2-}$·A (Figure 5d).

Fig. 7 displays the photofragment action spectra for production of the $PtCl_6^{2-}$, $[M-H]^-$ and $PtCl_5^-$ photofragments across the spectral range.[37] For both the $PtCl_6^{2-}$·U and $PtCl_6^{2-}$·T complexes (Figures 7a and 7b), $PtCl_6^{2-}$ is produced through a broad band from 4.4-5.4 eV, peaking at ~4.9 eV. The spectral profile of the $PtCl_5^-$ and $[M-H]^-$ ions closely matches that of $PtCl_6^{2-}$, indicating that this set of fragments have a common origin that is likely to correspond to ultrafast decay of a nucleobase-centred excited state and subsequent ground-state fragmentation. However, the behaviour of the $PtCl_6^{2-}$·C and $PtCl_6^{2-}$·A clusters is distinctive, and warrants further discussion.

For $PtCl_6^{2-}$·C (Figure 7c), only $PtCl_6^{2-}$ is observed (band peaks at ~4.9 eV), and this fragment has a relatively low intensity. No significant production of the accompanying $PtCl_5^-$ or $[M-H]^-$ fragments, which would be expected upon fragmentation of a "hot" ground state cluster, are seen through this band. This is perhaps unsurprising given the low intensity of the $PtCl_6^{2-}$ fragment (which was the dominant fragment obtained upon CID of the ground state cluster), as the $PtCl_5^-$ or $[M-H]^-$ fragments would be produced at even lower intensity than $PtCl_6^{2-}$ (Fig. 2b) and therefore may be below the detection limit of our experiment. We conclude that the nucleobase-centred deactivation pathway is significantly quenched in $PtCl_6^{2-}$·C, possibly due to competition from electron detachment from the initially-populated excited state.

For $PtCl_6^{2-}$·A, the only photofragment from the $PtCl_6^{2-}$, $[A-H]^-$ and $PtCl_5^-$ set of fragments is $[A-H]^-$. The fact that a $PtCl_6^{2-}$ photofragment is completely absent following photoexcitation of $PtCl_6^{2-}$·A indicates that ultrafast nucleobase-centred deactivation pathway is not competitive. Instead, it is clear that production of $[A-H]^-$ occurs through a lower-energy band peaked closer to 4.4 eV, and then increases towards higher photon energy. This behaviour would be expected for a photofragment produced by excitation of the LMCT transitions of $PtCl_6^{2-}$ within the cluster.[38] Any accompanying photofragments to $[A-H]^-$ (e.g. $PtCl_5^-$) must further fragment into $PtCl_4^-$ or $PtCl_3^-$. The spectra presented in the SI (Figs. S12 and S13) provide evidence for this.

Next we turn to the chloride anion-nucleobase photofragment, $M{\cdot}Cl^-$. This photofragment is discussed separately as it displays a distinctive photofragment action spectrum to the fragments discussed above. Action spectra for production of $M{\cdot}Cl^-$ are displayed in Fig. 8. For all four of the $PtCl_6^{2-}$·M clusters, the $M{\cdot}Cl^-$ displays a profile with a maximum intensity close to the low-energy spectral edge (~4.0 eV) that decreases towards zero by ~5.2 eV, before gradually starting to increase in intensity again towards higher energies. This profile is distinctive amongst the complete set of photofragments. The simplest route for

production of $M{\cdot}Cl^-$ is from ionic fragmentation, i.e. pathway [2], through direct photoexcitation of $PtCl_6^{2-}$ within the $PtCl_6^{2-}{\cdot}M$ cluster. As discussed in the introduction, bare gas-phase $PtCl_6^{2-}$ is known to produce $PtCl_5^-$ with a profile that peaks at ~4.5 eV before tailing down to zero at ~5.0 eV.[8] The $PtCl_5^-$ is thought to arise from photoinduced ionic fragmentation of $PtCl_6^{2-}$.[8] Since photoproduction of $M{\cdot}Cl^-$ from the $PtCl_6^{2-}{\cdot}M$ clusters occurs with the same general profile (i.e. decreasing towards a low photofragment intensity at ~5.2 eV), we assign the $M{\cdot}Cl^-$ photofragment as arising from photoinduced ionic fragmentation of the $PtCl_6^{2-}$ within the $PtCl_6^{2-}{\cdot}M$ cluster. We note that photoproduction of $Cl^-{\cdot}M$ from the cluster is red-shifted compared to photoproduction of $PtCl_5^-$ from bare $PtCl_6^{2-}$, possibly due to the LMCT transitions of $PtCl_6^{2-}$ in the $PtCl_6^{2-}{\cdot}M$ cluster being distributed across the range from 4.1-4.8 eV (Section 3.2).

Finally, we consider the $PtCl_4^-$ and $PtCl_3^-$ pair of photofragments (spectra are included in Section S4 of the SI), which display broadly similar action spectra for all of the clusters, with peaks at ~4.6 and >5.8 eV. From all of the photofragments observed for the $PtCl_6^{2-}{\cdot}M$ clusters, the spectral profiles of the $PtCl_4^-$ and $PtCl_3^-$ photofragments, most closely resemble the overall profiles of the photodepletion spectra. It is notable that $PtCl_5^-$ is not observed as an accompanying photofragment with the same spectral profile as $M{\cdot}Cl^-$ from the $PtCl_6^{2-}{\cdot}M$ clusters. This behaviour is reminiscent of the absence of $PtCl_5^-$ as an accompanying photofragment to $[M\text{-}H]^-$ for the $PtCl_6^{2-}{\cdot}A$ cluster. It is likely that $PtCl_5^-$ is produced as a vibrationally hot ion following LMCT excitation which dissociates with a high cross-section into $PtCl_4^-$ and $PtCl_3^-$. We conclude that the action spectra of $PtCl_4^-$ and $PtCl_3^-$ resemble the photodepletion spectra because these secondary ions are produced whenever $PtCl_5^-$ is formed; the conversion rate is low for nucleobase absorptions but has a near unit probability for LMCT transitions, reflecting the localisation of thermal energy.

4. CONCLUDING REMARKS

We have recently studied the photoelectron spectroscopy of the $PtCl_6^{2-}{\cdot}M$ clusters, employing 266 nm (4.66 eV) and 193 nm (6.424 eV) as the photodetachment energies.[20] The 266 nm spectrum of the $PtCl_6^{2-}{\cdot}A$ complex is particularly striking as it displays a very prominent broad featureless band that is indicative of a phenomenom termed "delayed electron detachment" in photodetachment spectroscopy.[40,41] Delayed electron detachment occurs when the photon employed excites an electronic transition of the system under study, rather than simply detaching an excess electron in a "direct" instantaneous photodetachment process. The delayed electron detachment observed for $PtCl_6^{2-}{\cdot}A$ in its 4.66 eV photoelectron spectrum indicates that

one-photon excitation accesses excited states that are sufficiently long-lived to allow coupling to the electron detachment continuum and subsequent autodetachment. This process appears to have a significant impact on the photochemistry of $PtCl_6^{2-}$·A at this wavelength, making the action spectra of the photofragments distinctive for this cluster. The detailed photophysics of gas-phase nucleobase molecules is a topic of continuing high-interest, and there have been a number of recent studies exploring how adjacent negative charge modifies the deactivation pathways of adenine. Further characterisation of the detailed excited states and decay pathways available to the $PtCl_6^{2-}$·A cluster requires time-resolved photodetachment spectroscopy.[42] Such measurements have the potential to provide new insight into the intrinsic nucleobase decay dynamics.

The 266 nm photoelectron spectra of the $PtCl_6^{2-}$·T and $PtCl_6^{2-}$·C clusters also display "delayed electron detachment" (strongest for $PtCl_6^{2-}$·T), although for the $PtCl_6^{2-}$·U cluster, the delayed detachment signal is very small. These observations from the photoelectron spectroscopy study are in line with our general observations of the relative intensities of summed electron detachment photofragments, with electron detachment fragments being more prominent for the $PtCl_6^{2-}$·A and $PtCl_6^{2-}$·T clusters. If we compare $PtCl_6^{2-}$·A and $PtCl_6^{2-}$·T, the fact that $PtCl_6^{2-}$·T produced $PtCl_6^{2-}$ (formed via a cluster fission process) as a significant photofragment indicates that branching between the electron detachment decay pathway and the ultrafast (nucleobase-centred) decay to the hot electronic ground state is more comparable. In $PtCl_6^{2-}$·A, the electron detachment channel dominates strongly. Time-resolved photodetachment spectroscopy is again needed to more fully characterise the novel photophysics observed here.

In previous related work, we have explored the photophysics and photochemistry of clusters composed of nucleobases bound to the $Pt(CN)_4^{2-}$ and $Pt(CN)_6^{2-}$ dianions, e.g. $Pt(CN)_4^{2-}$·M.[5-7] The overall photochemistry of these clusters is simpler than the hexachloroplatinate clusters studied here, since the nucleobase-centred chromophores are considerably stronger than any on $Pt(CN)_4^{2-}$ and $Pt(CN)_6^{2-}$ over the spectral range covered. Focusing on the $Pt(CN)_4^{2-}$·M clusters, the laser induced photochemistry fell into two classes dependent on the excitation wavelength. In the region between ~4.4-5.2 eV, excitation of the primarily nucleobase-centred chromophore leads to a photo-induced proton transfer reaction from the nucleobase to the platinum complex, whereas at excitation energies above ~5.2 eV, photodetachment begins to dominate. Both of these photo-induced processes have the capacity to destroy nucleotides (or DNA) that the platinum complexes are bound to, either through the proton-transfer pathways or due to photodetachment releasing destructive free electrons into the vicinity of a

nucleobase.[43,44] For the $PtCl_6^{2-}$·M clusters studied here, we see similar partitioning into two photochemical regions: A lower energy region (<5.2 eV) where the $PtCl_6^{2-}$ moiety is photolysed, ejecting Cl^- bound to the nucleobase (with potential to initiate a proton-transfer process) and a higher-energy region (>5.2 eV) where electron photodetachment dominates. These experiments demonstrate how selective photoexcitation can drive distinctive photodecay channels for a model photo-pharmaceutical. Such studies provide critical benchmarking data for developing QM/MM methodologies for modelling photoactive metal complex-biomolecule interactions and have the potential to provide a route for facile screening of possible photopharmaceuticlas.

ACKNOWLEDGEMENTS

This work was supported through the European Research Council grant 208589-BIOIONS. We are grateful to the STFC for the provision of equipment from the EPSRC Laser Loan Pool (Grant # 13250030), as well as the University of York and Department of Chemistry at the University of York for provision of funds for the Horizon OPO laser system. We also thank the EPSRC UK NSCCS at Imperial College London for the award of grant CHEM 798.

REFERENCES

1. N. A. Smith and P. J. Sadler, *Phil. Trans. R. Soc. A.*, 2013, **371**, 20120519.
2. F. S. Mackay, J. A. Woods, P. Heringová, J. Kašpárková, A. M. Pizarro, S. A. Moggach, S. Parsons, V. Brabec and P. J. Sadler, *Proc. Natl. Acad. Sci. U S A.*, 2007, **104**, 20743.
3. E. Shaili, *Sci. Prog*., 2014, **97**, 20.
4. T. Gianferrara, I. Bratsos and E. Alessio, *Dalton Trans.*, 2009, **37**, 7588.
5. A. Sen, T. F. M. Luxford, N. Yoshikawa and C. E. H. Dessent, *Phys. Chem. Chem. Phys.*, 2014, **16**, 15490.
6. A. Sen and C. E. H. Dessent, *J. Chem. Phys*., 2014, **141**, 241101.
7. A. Sen and C. E. H. Dessent, *J. Phys. Chem. Lett*., 2014, ***5***, 3281.
8. S. H. Kaufman, J. M. Weber and M. Pernpointner, *J. Chem. Phys.*, 2013, **139**, 194310.
9. X. B. Wang and L. S. Wang, *J. Chem. Phys.*, 1999, **111**, 4497.
10. T. Sommerfeld, S. Feuerbacher, M. Pernpointner and L. S. Cederbaum, *J. Chem. Phys.*, 2003, **118**, 1747.
11. M. Pernpointer, T. Rapps, and L. S. Cederbaum, *J. Chem. Phys.*, 2009, **131**, 044322.
12. E. M. Glebov, I. P. Pozdnyakov, V. F. Plyusnin and I. Khmelinskii, *J. Photochem. Photobiol. C*, 2015, **24**, 1.
13. M. Sakamoto, M. Fujistuka and T. Majima, *J. Photochem. Photobiol. C*, 2009, **10**, 33.
14. W. Macyk and H. Kisch, *Chem. Eur. J.*, 2001, **7**, 1862.
15. C. Harris and P. V. Kamat, *ACS Nano*, 2010, **4**, 7321.
16. C. T. Middleton, K. de La Harpe, C. Su, Y. K. Law, C. E. Crespo Hernandez and B. Kohler, *Ann. Rev. Phys. Chem.,* 2009, **60**, 217.
17. W. J. Schreier, P. Gilch and W. Zinth, *Ann. Rev. Phys. Chem.,* 2015, **66**, 497.
18. K. Kleinermanns, D. Nachtigallov and M. S. de Vries, *Int. Rev. Phys. Chem.,* 2013, **32**, 308.
19. R. Improta, F. Santoro and L. Blancafort, *Chem. Rev.,* 2016, **116**, 3540.
20. A. Sen, E. M. Matthews, G. L. Hou, X. B. Wang and C. E. H. Dessent, *J. Chem. Phys.*, 2015, **143**, 184307.
21. W. E. Boxford and C. E. H. Dessent, *Phys. Chem. Chem. Phys.*, 2006, **8**, 5151.
22. T. F. M. Luxford, E. M. Milner, N. Yoshikawa, C. Bullivant and C. E. H. Dessent, *Chem. Phys. Lett.*, 2013, **577**, 1.
23. A. De Fusco, J. Ivanic, M. W. Schmidt and M. S. Gordon, *J. Phys. Chem. A*, 2011, **115**, 4574.
24. F. Santoro, V. Barone and R. Improta, *J. Comput. Chem.*, 2008, **29**, 957.

25. A. Y. Sokolov and H. F. Schaefer, III, *Dalton Trans*., 2011, **40**, 7571.

26. M. J. Frisch, G. W. Trucks, H. B. Schlegel, G. E. Scuseria, M. A. Robb, J. R. Cheeseman, G. Scalmani, V. Barone, B. Mennucci, G. A. Petersson, H. Nakatsuji, M. Caricato, X. Li, H. P. Hratchian, A. F. Izmaylov, J. Bloino, G. Zheng, J. L. Sonnenberg, M. Hada, M. Ehara, K. Toyota, R. Fukuda, J. Hasegawa, M. Ishida, T. Nakajima, Y. Honda, O. Kitao, H. Nakai, T. Vreven, J. A. Montgomery, Jr., J. E. Peralta, F. Ogliaro, M. Bearpark, J. J. Heyd, E. Brothers, K. N. Kudin, V. N. Staroverov, R. Kobayashi, J. Normand, K. Raghavachari, A. Rendell, J. C. Burant, S. S. Iyengar, J. Tomasi, M. Cossi, N. Rega, J. M. Millam, M. Klene, J. E. Knox, J. B. Cross, V. Bakken, C. Adamo, J. Jaramillo, R. Gomperts, R. E. Stratmann, O. Yazyev, A. J. Austin, R. Cammi, C. Pomelli, J. W. Ochterski, R. L. M artin, K. Morokuma, V. G. Zakrzewski, G. A. Voth, P. Salvador, J. J. Dannenberg, S. Dapprich, A. D. Daniels, Ö. Farkas, J. B. Foresman, J. V. Ortiz, J. Cioslowski, and D. J. Fox, Gaussian 09 (Revision D.01), Gaussian, Inc., Wallingford, CT, 2009.

27. Y. Zhao and D. G. Truhlar, *Theor. Chem. Account,* 2008, **120**, 215.

28. R. Krishnan, J. S. Binkley, R. Seeger, and J. A. Pople, *J. Chem. Phys.*, 1980, **72**, 650.

29. A. D. McLean and G. S. Chandler, *J. Chem. Phys.*, 1980, **72**, 5639; F. Weigend and R. Ahlrichs, P*hys. Chem. Chem. Phys.*, 2005, **7**, 3297; F. Weigend, *Phys. Chem. Chem. Phys.*, 2006, **8**, 1057; D. Andrae, U. Häussermann, M. Dolg, H. Stoll, and H. Preuss, *Theor. Chim. Acta.*, 1990, **77**, 123.

30. L. B. Clark, G. G. Pescheland and I. Tinoco, Jr., *J. Phys. Chem.*, 1965, **69**, 3615.

31. M. Barbatti, A. J. A. Aquino, and H. Lischka, *Phys. Chem. Chem. Phys.*, 2010, **12**, 4959.

32. M. K. Shukla, and J. Leszczynski, *J. Comput. Chem.*, 2004, **25**, 768.

33. E. Nir, M. Muller, L. I. Grace and M. S. de Vries, *Chem. Phys. Lett.,* 2002, **355**, 59.

34. Production of the $PtCl_3^-$ photofragment from $PtCl_6^{2-}\cdot A$ has been calculated to be endothermic by >3.5 eV. (Calculated by comparing the difference in the computed SCF energies between $PtCl_6^{2-}\cdot A$ and $PtCl_3^-$, $A\cdot Cl^-$, and two Cl· radicals. All structures and energies were calculated using the method described in Section 2. Frequency calculations were performed on the optimised structures to show that they are minima.) Thus, both the internal energy and timescale required to dissociate the excited $[PtCl_6^{2-}\cdot A]^*$ cluster into a nucleobase and three Cl atoms (along with the ionic photofragment) are unlikely to be available in the electronic excited state.

35. A. S. Chatterley, C. W. West, V. G. Stavros and J. R. R. Verlet, *Chem. Sci.*, 2014, **5**, 3963.

36. J. C. Marcum, A. Halevi and J. M. Weber, *Phys. Chem. Chem. Phys.,* 2009, **11**, 1740; B. Liu, P. Hvelplund, S. B. Nielsen and S. Tomita, *Phys. Rev. A.*, 2006, **74**, 052704.

37. The $PtCl_5^-$ ion was observed in both laser on and laser off measurements. For the cytosine and adenine clusters, the intensity of $PtCl_5^-$ was similar in the laser on and laser of measurements, so that it is not a significant photofragment (*i.e.* it is not a true photofragment in the MS presented in Figs. 7c and 7d). For the uracil and thymine clusters, the intensity of $PtCl_5^-$ was adjusted in the photofragment action spectra (Figs. 5a and 5b) to remove the background contribution of this ion, so that the plotted spectra are for the photofragment.

38. It is also possible that the $[A\text{-}H]^-$ photofragment is produced via an excited state hydrogen transfer process in adenine.[39]

39. A. L. Sobolewski and W. Domcke, *J. Phys. Chem. A*, 2007, **111**, 11725.

40. E. E. B. Campbell and R. D. Levine, *Annu. Rev. Phys. Chem.,* 2000*,* **51**, 65: H. Häkkinen, B. Yoon, U. Landman, X. Li, H. J. Zhai, and L. S. Wang, *J. Phys. Chem. A.*, 2003, **107**, 6168.

41. K. Matheis, L. Joly, R. Antoine, F. Lépine, C. Bordas, O. T. Ehrler, A. R. Allouche, M. M. Kappes, and P. Dugourd, *J. Am. Chem. Soc.,* 2008*,* **130**, 15903.

42. J. R. R. Verlet, D. A. Horke, and A. S. Chatterley, *Phys. Chem. Chem. Phys.,* 2014, **16**, 15043.

43. J. Simons, *Acc. Chem. Res.,* 2006, **39**, 772.

44. Q. H. Bao, Y. F. Chen, Y. Zeng and L. Sanche, *J. Phys. Chem. C.*, 2014, **118**, 15516.

TABLES

Table 1: Low-energy CID results for the $PtCl_6^{2-}$·M, M = A, C, T, U clusters, including $E_{1/2}$ fragmentation energies and CID fragment ions.[a,b]

Cluster	$E_{1/2}$	Product ions
$PtCl_6^{2-}$·A	6.49	$PtCl_6^{2-}$, $PtCl_5^-$, A·Cl^-, [A-H]$^-$
$PtCl_6^{2-}$·C	6.17	$PtCl_6^{2-}$, $PtCl_5^-$, C·Cl^-
$PtCl_6^{2-}$·T	6.50	$PtCl_6^{2-}$, $PtCl_5^-$, T·Cl^-
$PtCl_6^{2-}$·U	6.64	$PtCl_6^{2-}$, $PtCl_5^-$, U·Cl^-, [U-H]$^-$

[a] $E_{1/2}$ values are for 50% depletion of the parent cluster.
[b] Product ions are listed in order of decreasing fragment ion intensity.

Table 2: Calculated transition energies and oscillator strengths of $PtCl_6^{2-}$·U from TD-DFT calculations with the M06-2X functional.[a]

Transition Energy (eV)	Oscillator Strength
$PtCl_6^{2-}$ LMCT Transitions	
4.15	0.0116
4.17	0.0142
4.27	0.0135
4.59	0.0216
4.62	0.0492
4.63	0.0300
4.66	0.1352
4.69	0.1632
4.79	0.1142
5.93	0.0367
Uracil π and $PtCl_6^{2-}$ Orbitals → Uracil π* Transitions[b]	
5.28	0.2899
5.75	0.0240

[a] Only transitions with oscillator strength >0.005 are listed.

[b] Uracil π orbitals have a minor electronic delocalisation to the $PtCl_6^{2-}$ moiety.

FIGURES

Figure 1: Negative ion ESI-MS of a solution of the sodium salt of $PtCl_6^{2-}$ with the nucleobase thymine.

Figure 2: % Fragmentation decay curves for a) $PtCl_6^{2-}$·A, b) $PtCl_6^{2-}$·C, c) $PtCl_6^{2-}$·T and d) $PtCl_6^{2-}$·U upon low energy CID. Onset plots for production of the associated fragment ions are also shown. Typical experimental errors (obtained for repeat runs) were ±3%.

Figure 3: Calculated excitation energies of the $PtCl_6^{2-}$·U from TDDFT calculations with the M06-2X functional. The oscillator strengths of individual transitions are given by the vertical bars. The full line spectrum represents a convolution of the calculated spectrum with a Gaussian function (0.333 eV HWHM).

Figure 4: Photodepletion (absorption) spectra of (a) $PtCl_6^{2-}$·U, (b) $PtCl_6^{2-}$·T, (c) $PtCl_6^{2-}$·C and (d) $PtCl_6^{2-}$·A across the region 4.0 – 5.8 eV. The solid lines are five point adjacent averages of the data points.

Figure 5: Photofragmentation mass spectra (laser on) of the $PtCl_6^{2-}$·M clusters obtained at 4.77 eV (270 nm) where M = a) uracil, b) thymine, c) cytosine, d) adenine.[30] The parent peak is denoted by the *.

Figure 6: Photofragment action spectra of sum of the electron detached fragments ($PtCl_6^-$, $PtCl_6^-$·A and $[PtCl_5(A\text{-}H)]^-$) of the $PtCl_6^{2-}$·M clusters over the range 4.0 – 5.8 eV. [30] The solid lines are five point adjacent averages of the data points.

Figure 7: Photofragment action spectra of the $PtCl_6^{2-}$ (red circles), $PtCl_5^-$ (blue circles) and $[M\text{-}H]^-$ (black circles) photofragments produced from a) $PtCl_6^{2-}$·U, b) $PtCl_6^{2-}$·T, c) $PtCl_6^{2-}$·C and d) $PtCl_6^{2-}$·A. Action spectra of $[M\text{-}H]^-$ for the

cytosine cluster and $PtCl_6^{2-}$ for the adenine cluster are not included due to their low production. $PtCl_5^-$ photoproduction intensities are corrected for trapping impurities. The solid lines are five point adjacent averages of the data points.

Figure 8: Photofragment action spectra of $Cl^-{\cdot}M$ produced from a) $PtCl_6^{2-}{\cdot}U$, b) $PtCl_6^{2-}{\cdot}T$, c) $PtCl_6^{2-}{\cdot}C$ and d) $PtCl_6^{2-}{\cdot}A$. The solid lines are five point adjacent averages of the data points.

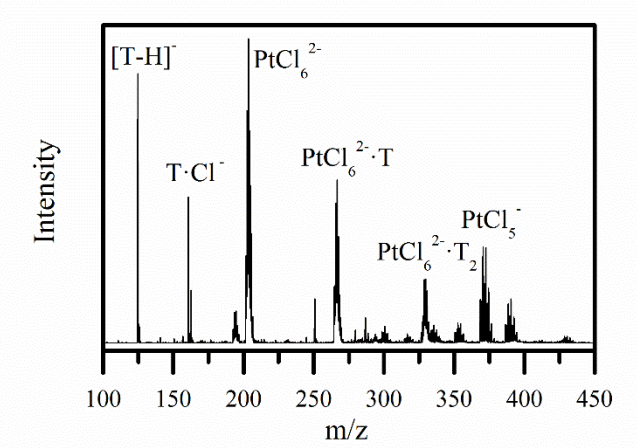
[T-H]-
PtCl6 2-
T·Cl-
PtCl6 2-·T
PtCl5-
PtCl6 2-·T2
Intensity
100
150
200
250
300
350
400
450
m/z

Figure 1

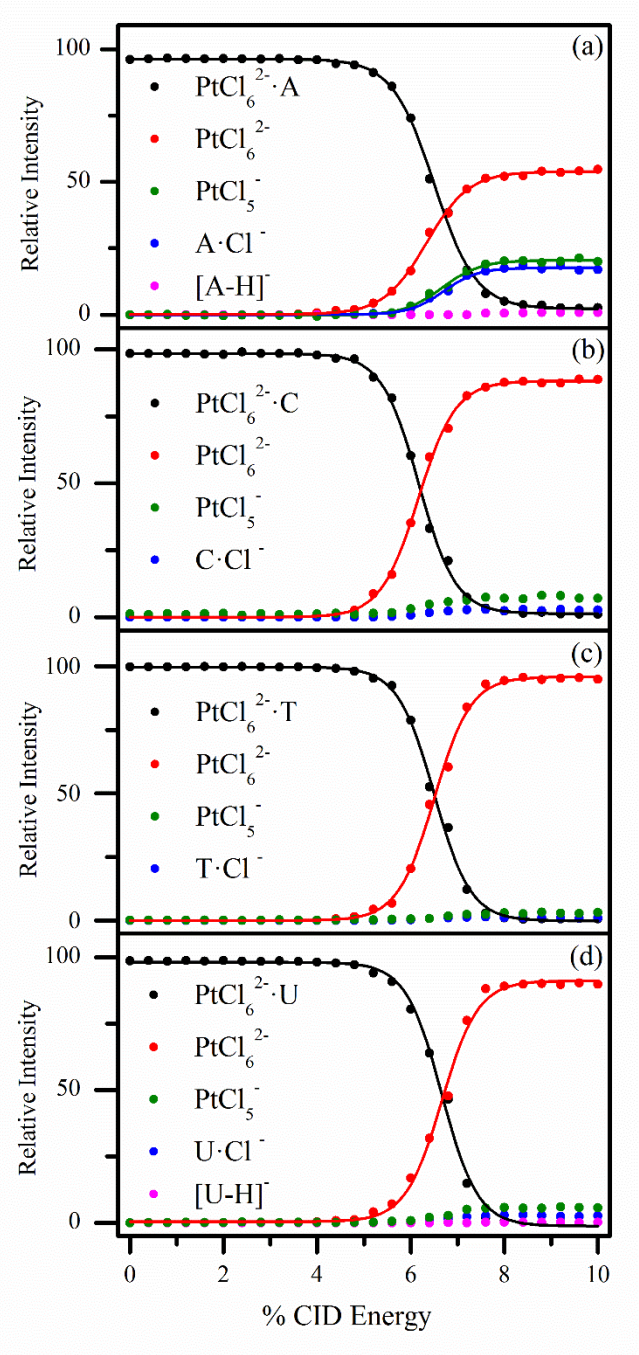
(a)
$PtCl_6^{2-}$·A
$PtCl_6^{2-}$
$PtCl_5^-$
A·Cl$^-$
[A-H]$^-$
(b)
$PtCl_6^{2-}$·C
$PtCl_6^{2-}$
$PtCl_5^-$
C·Cl$^-$
(c)
$PtCl_6^{2-}$·T
$PtCl_6^{2-}$
$PtCl_5^-$
T·Cl$^-$
(d)
$PtCl_6^{2-}$·U
$PtCl_6^{2-}$
$PtCl_5^-$
U·Cl$^-$
[U-H]$^-$
Relative Intensity
100
50
0
0
2
4
6
8
10
% CID Energy

Figure 2

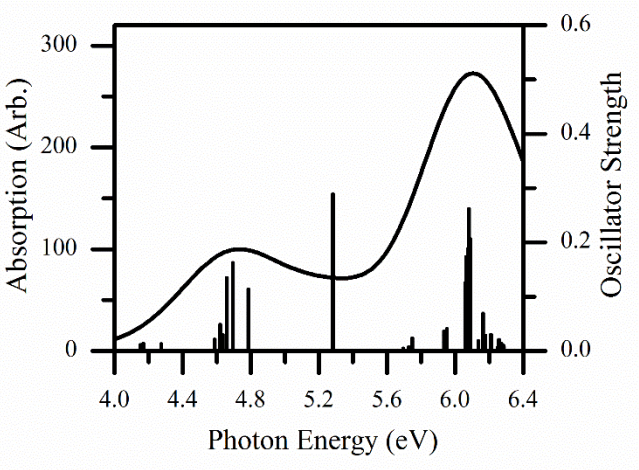
Absorption (Arb.)
Oscillator Strength
Photon Energy (eV)
300
200
100
0
0.6
0.4
0.2
0.0
4.0
4.4
4.8
5.2
5.6
6.0
6.4

Figure 3

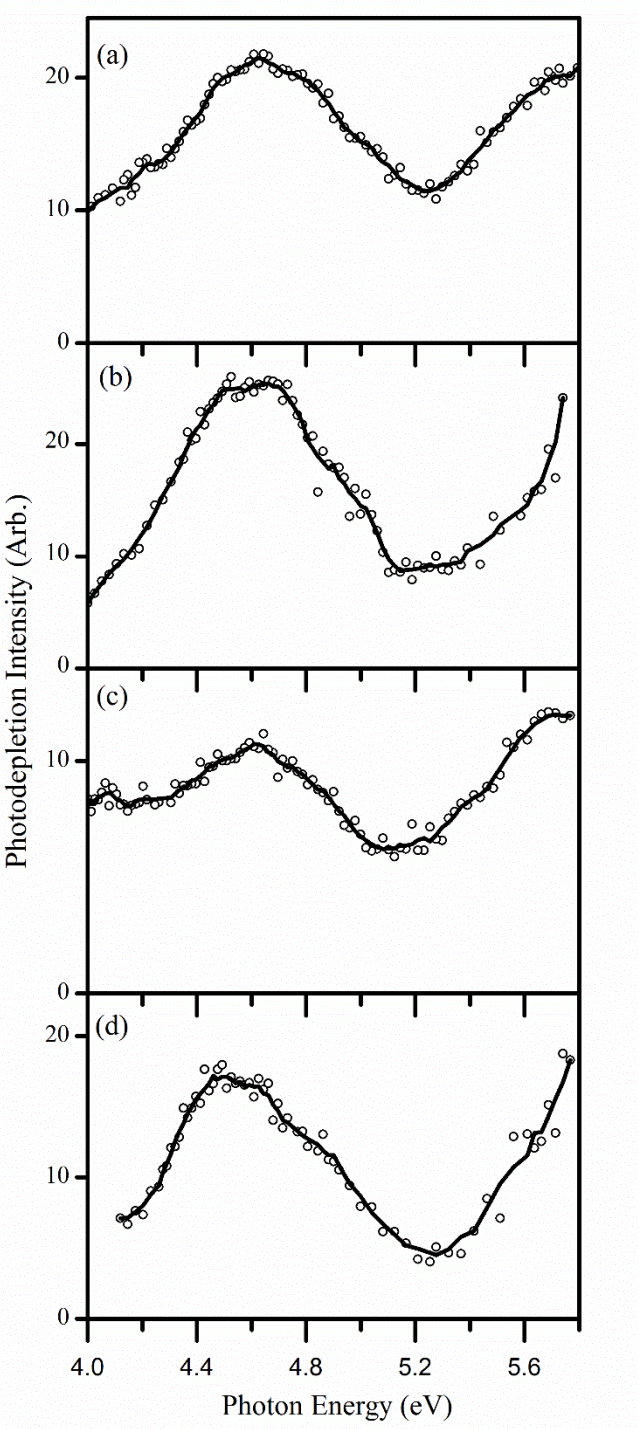
(a)
(b)
(c)
(d)
Photodepletion Intensity (Arb.)
Photon Energy (eV)
4.0
4.4
4.8
5.2
5.6
0
10
20

Figure 4

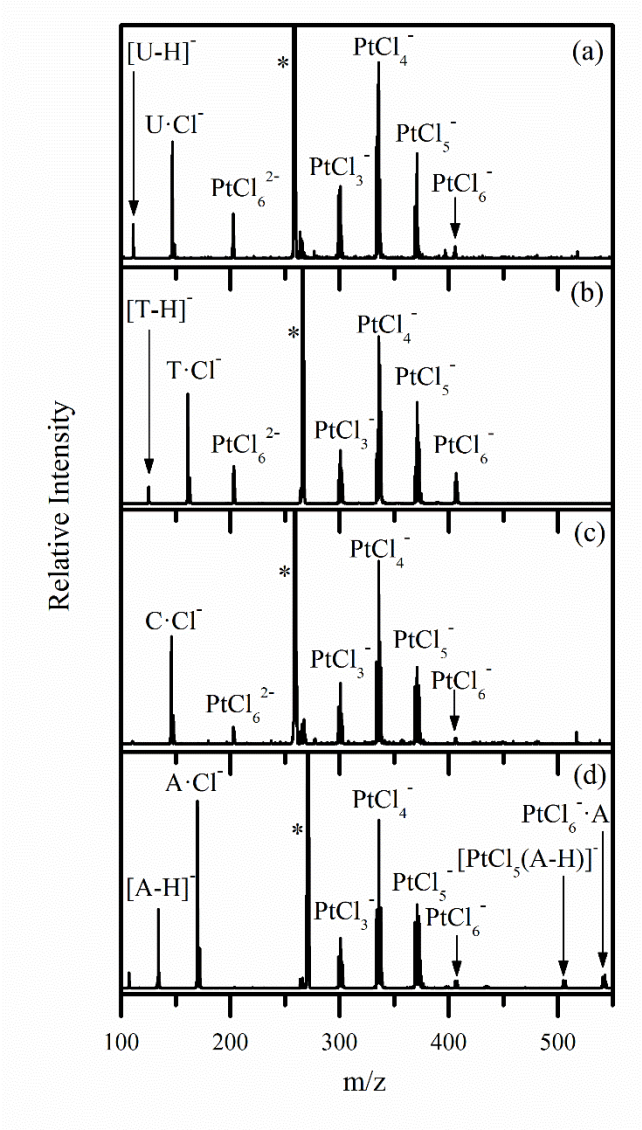
[U-H]-
U·Cl-
PtCl6 2-
PtCl4-
PtCl3-
PtCl5-
PtCl6-
(a)
[T-H]-
T·Cl-
(b)
C·Cl-
(c)
A·Cl-
[A-H]-
PtCl6-·A
[PtCl5(A-H)]-
(d)
*
Relative Intensity
100
200
300
400
500
m/z

Figure 5

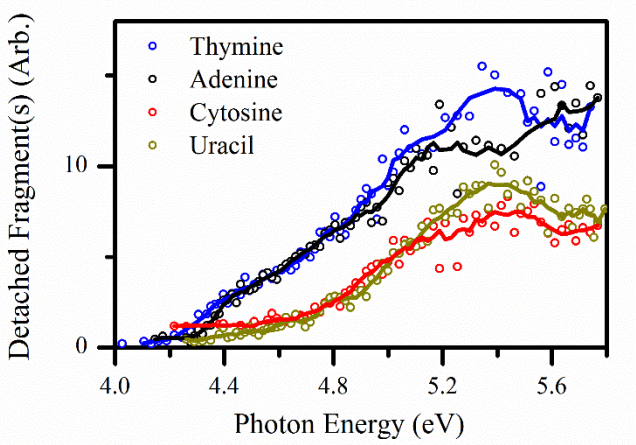
Detached Fragment(s) (Arb.)
Thymine
Adenine
Cytosine
Uracil
10
0
4.0
4.4
4.8
5.2
5.6
Photon Energy (eV)

Figure 6

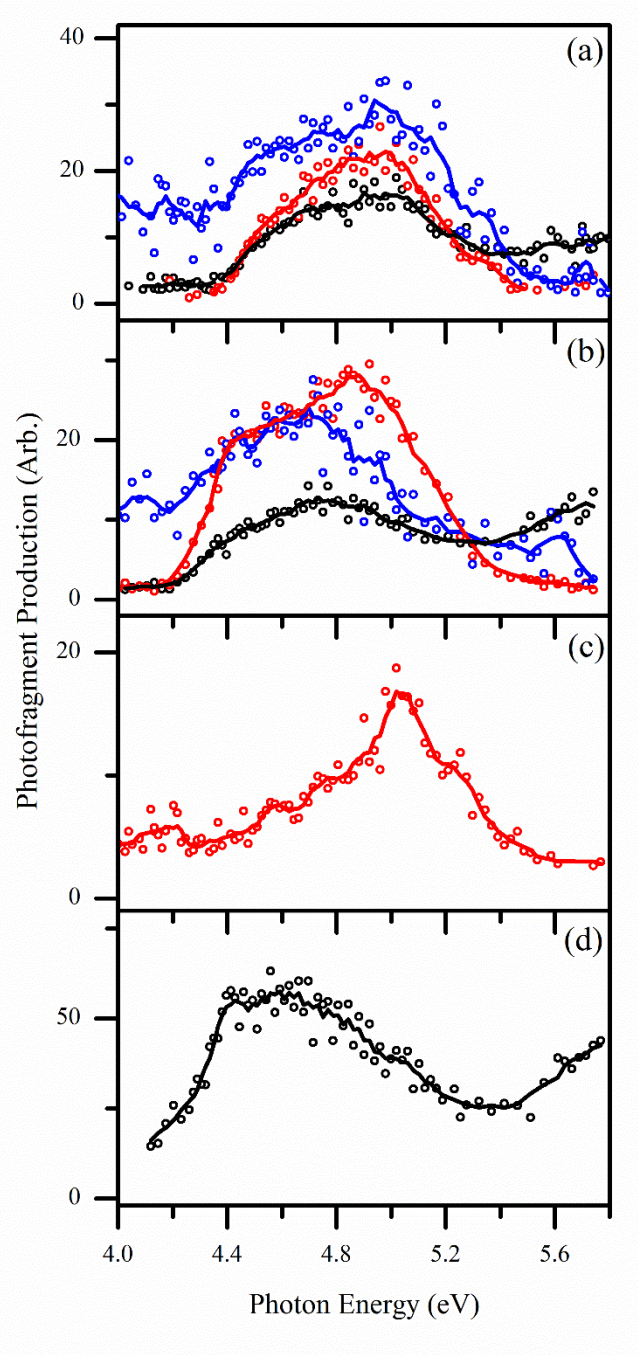
(a)
(b)
(c)
(d)
40
20
0
20
0
20
0
50
0
Photofragment Production (Arb.)
4.0
4.4
4.8
5.2
5.6
Photon Energy (eV)

Figure 7

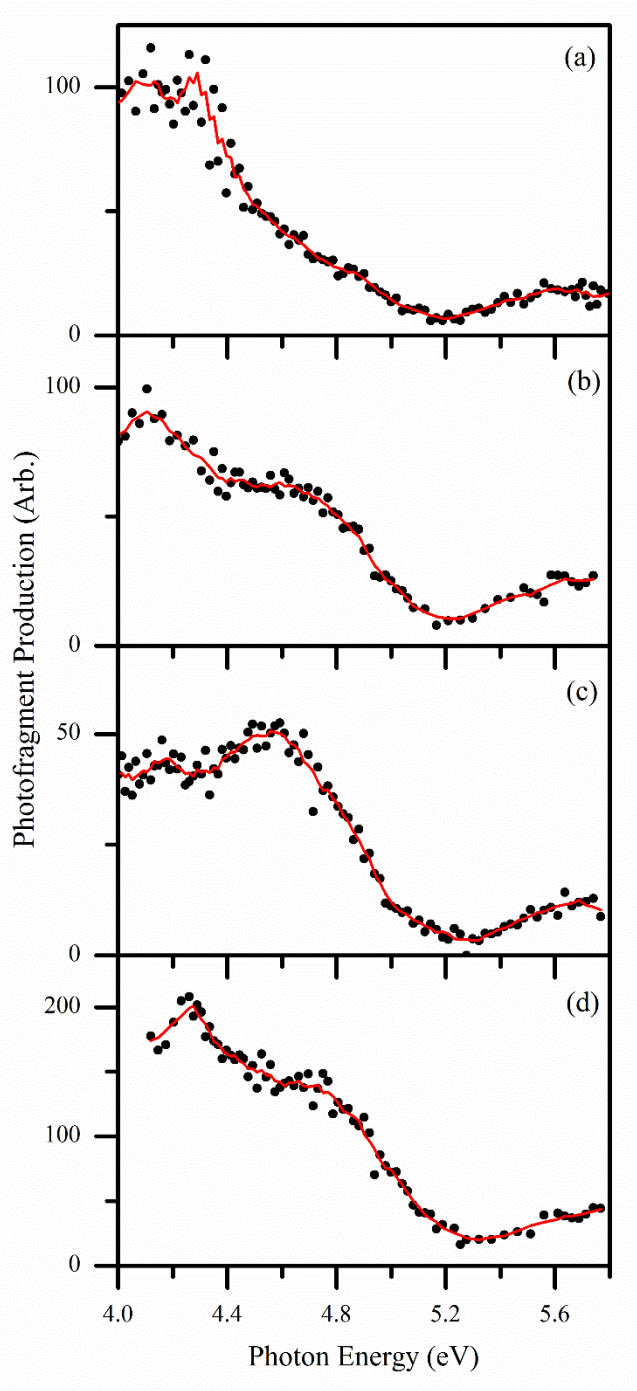
(a)
(b)
(c)
(d)
100
0
100
0
50
0
200
100
0
Photofragment Production (Arb.)
4.0
4.4
4.8
5.2
5.6
Photon Energy (eV)

Figure 8